Proposal for observing non-Abelian statistics of Majorana-Shockley fermions in an optical lattice

Dong-Ling Deng,[1,2] Sheng-Tao Wang,[1,2] Kai Sun,[1] and Lu-Ming Duan[1,2]
[1]*Department of Physics, University of Michigan, Ann Arbor, Michigan 48109, USA*
[2]*Center for Quantum Information, IIIS, Tsinghua University, Beijing 100084, People's Republic of China*
(Received 22 November 2014; revised manuscript received 3 March 2015; published 23 March 2015)

Besides the conventional bosons and fermions, in synthetic two-dimensional (2D) materials there could exist more exotic quasiparticles with non-Abelian statistics, meaning that the quantum states in the system will be transformed by noncommuting unitary operators when we adiabatically braid the particles one around another. Here, we propose an experimental scheme to observe non-Abelian statistics with cold atoms in a 2D optical lattice. We show that the Majorana-Schockley modes associated with line defects can be braided with non-Abelian statistics through adiabatic shift of the local potentials. We also demonstrate that the braiding operations are robust against typical experimental imperfections and the readout of topological qubits can be accomplished by local measurement of the atom number.

DOI: 10.1103/PhysRevB.91.094513 PACS number(s): 67.85.−d, 03.65.Vf, 03.67.Lx, 05.30.Rt

I. INTRODUCTION

Majorana fermions are exotic particles which, unlike electrons and positrons, constitute their own antiparticles [1] and exhibit non-Abelian statistics [2]. They are important not only because of their fundamental role in condensed matter [2–4] and high energy physics [1,5], but also because of their promising practical applications in topological quantum information processing tasks, such as the synthesis of a fault-tolerant quantum computer [6,7] or a certifiable random number generator [8]. However, in spite of extensive exciting progresses [9–16], the unambiguous detection of Majorana fermions and the probe of their non-Abelian statistical properties remain one of the foremost ongoing goals in current physics.

Laser controlled cold atoms provide a powerful experimental platform to realize exotic states of matter [17–19]. Several proposals have been made to observe non-Abelian statistics based on control of vortex states in a $p+ip$ superfluid [20–22]. A vortex in a $p+ip$ superfluid of odd vorticity traps a zero-energy mode corresponding to a Majorana fermion. The Majorana fermions in different vortices are found to obey non-Abelian statistics [23–25]. An intriguing proposal has been made to braid the vortex Majorana fermions in a cold atomic gas by a focused laser beam [21,22]. An experimental implementation of this proposal, however, is still challenging for several reasons: first, besides the Majorana mode a vortex also traps a number of other in-gap states [21]. The small energy difference between these states and the zero-energy Majorana mode sets a tough requirement for the relevant energy and time scales. Second, moving the vortex by a focused laser beam may change its trapped modes, and a quantitative understanding of this process is still lacking. Finally, a natural way to realize the $p+ip$ superfluid is based on the p-wave Feshbach resonance [26], but the latter is difficult to stabilize in free space [27,28]. Very recently, another nice idea has been suggested to braid Majorana modes associated with dislocations in an optical lattice [29]. Insertion of dislocations requires a change of structure of the optical lattice, which is experimentally challenging and yet to be demonstrated.

In this paper, we propose an experimental scheme to observe non-Abelian statistics with cold atoms in an optical lattice in a vortex-free configuration. A p-wave superfluid based on the Feshbach resonance could be stabilized in an optical lattice due to the quantum Zeno effect [28,30]. The recent remarkable experimental advance has allowed single-site addressing in a two-dimensional (2D) optical lattice [31–35]. With this capability, we can create a line defect in a 2D lattice simply by shifting the chemical potential along the line. Different from dislocations, this line defect requires no structure change of the underlying optical lattice and is ready to be implemented in current experiments [31–35]. Recently, it was found that a pair of zero-energy modes shall emerge at the edges of this line defect [36] by the Shockley mechanism [37]. The exchange statistics of these modes, however, remains unresolved [36]. A challenge that may render the statistics uncertain and difficult to detect is the fact that braiding of these modes will inevitably involve conjoining and cutting the line defects hosting them. Motivated by recent works on braiding of nanowires [38], here we utilize exact numerical methods to demonstrate that the Majorana-Shockley modes associated with these line defects in a 2D superfluid obey non-Abelian statistics and their braiding can be achieved by tuning of only the local chemical potential. This tuning is significantly simpler compared with the braiding of nanowires [38] or dislocations [29], which requires site-by-site tuning of the pairing interaction and the tunneling rates [38,39]. We also demonstrate robustness of the braiding operation against practical noise and propose a scheme to measure the topological qubits using local measurement of the atom number. The proposed scheme fits well with the state of the art of the experimental technology in a 2D optical lattice [31–35].

II. SYSTEM AND HAMILTONIAN

We consider cold atoms in a 2D optical lattice, which are prepared into the $p+ip$ superfluid phase. This superfluid phase can be achieved, for instance, through the p-wave Feshbach resonance [26]. The instability associated with the p-wave Feshbach resonance in free space [27] could be overcome in an optical lattice through the quantum Zeno effect [28]. Alternatively, an effective $p+ip$ superfluid phase for cold atoms can also be achieved by a combination of the s-wave Feshbach resonance and the light induced spin-orbital coupling [22,40,41].

In the momentum $\mathbf{k}$ space, the Bogoliubov–de Gennes (BdG) Hamiltonian describing the $p+ip$ superfluid phase on a square optical lattice has the form $H=\sum_{\mathbf{k}}\psi_{\mathbf{k}}^{\dagger}\mathcal{H}(\mathbf{k})\psi_{\mathbf{k}}$, with $\psi_{\mathbf{k}}^{\dagger}=(c_{\mathbf{k}}^{\dagger},c_{-\mathbf{k}})$ and

$$\mathcal{H}(\mathbf{k})=d_x(\mathbf{k})\sigma^x+d_y(\mathbf{k})\sigma^y+d_z(\mathbf{k})\sigma^z, \tag{1}$$

where $d_x(\mathbf{k})=\Delta\sin k_x a$, $d_y(\mathbf{k})=\Delta\sin k_y a$, $d_z(\mathbf{k})=\mu-J(\cos k_x a+\cos k_y a)$, $\sigma^{x,y,z}$ denote the Pauli matrices, a is the lattice constant, μ is the chemical potential, J is the neighboring hopping rate, and Δ is the pairing strength. The topological property of this Hamiltonian is characterized by the first Chern number $C_1=-\frac{1}{2\pi}\int_{\mathrm{BZ}}dk_x dk_y F_{xy}(\mathbf{k})$ with the Berry curvature $F_{xy}(\mathbf{k})=\partial_{k_x}A_y(\mathbf{k})-\partial_{k_y}A_x(\mathbf{k})$ and the Berry connection $A_\nu(\mathbf{k})=\langle u_-(\mathbf{k})|i\partial_{k_\nu}|u_-(\mathbf{k})\rangle$ $(\nu=x,y)$, where $|u_-(\mathbf{k})\rangle$ denotes the lower band Bloch eigenstate of $\mathcal{H}(\mathbf{k})$ and the integration in C_1 is over the first Brillouin zone (BZ). The phase of the Hamiltonian H is topologically nontrivial with $C_1=\mathrm{sgn}(\mu)$ in the parameter regime $0<|\mu|<2J$ (taking Δ as the energy unit) and topologically trivial with $C_1=0$ when $|\mu|>2J$. A topological phase transition occurs at $|\mu|=2J$.

III. CREATION AND BRAIDING OF MAJORANA-SHOCKLEY FERMIONS

With single-site addressing, the potential shift of each lattice site can be individually adjusted in experiments [31–35]. We create a line defect in a 2D optical lattice by tuning the chemical potential μ_d along a chain of atoms to make it different from that of the background lattice (denoted by μ_0) so that they reside in topologically distinct phases [illustrated in Fig. 1(a)]. For a certain range of μ_d that depends on μ_0, a pair of zero-energy Majorana-Shockley fermion (MSF) modes appear at the two edges of the line defect [36]. We choose μ_0 in the topologically trivial phase with $\mu_0>2J$ so that there are no other zero-energy modes on the boundary of the finite 2D lattice.

Under a typical size of the 2D optical lattice with a line defect, we solve exactly the eigenmodes of the Hamiltonian (1) under open boundary conditions, and the eigenspectrum is shown in Fig. 1(b). Clearly, there are a pair of zero-energy MSF modes that are separated from other defect modes and bulk states by a minimum gap about J. The MSFs are described by anticommuting real fermion operators γ_j with $\gamma_j=\gamma_j^{\dagger}$ and $\gamma_j\gamma_k+\gamma_k\gamma_j=2\delta_{jk}$. A pair of MSF modes γ_1 and γ_2 together represents a conventional fermion mode $c_m=(\gamma_1+i\gamma_2)/2$, with the eigenstates of $c_m^{\dagger}c_m=\frac{1}{2}(i\gamma_1\gamma_2+1)$ encoding a topological qubit. The eigenfunctions of the MSF modes γ_1 and γ_2 are shown in Fig. 1(c), which are well localized at the edges of the line defect.

IV. PROOF OF NON-ABELIAN STATISTICS

To examine the exchange statistic of the MSF modes, we adiabatically deform the line defect with steps shown in Figs. 2(a)–2(f). Each step is achieved through site-by-site tuning of the chemical potential from μ_d to μ_0 (to shorten the line defect) or from μ_0 to μ_d (to extend the line defect). We simulate the time evolution of the MSF modes in the Heisenberg picture. Under the adiabatic evolution, the

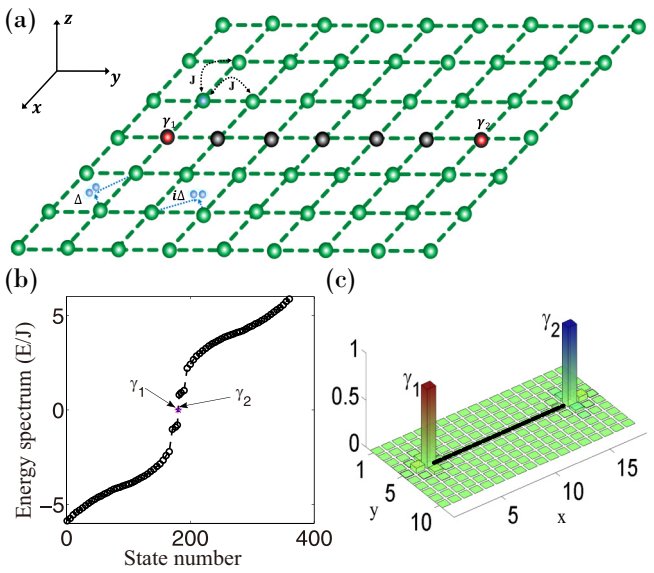

FIG. 1. (Color online) Creation and manipulation of the MSFs in an optical lattice. (a) Cold fermionic atoms are loaded into a 2D optical lattice. J and Δ denote the nearest neighbor hopping rate and pairing strength. A line defect with different local chemical potential binds two zero-energy MSFs γ_1 and γ_2 (red circles) at its edges. (b) Energy spectrum of the Hamiltonian H on a square lattice of size $18a\times 10a$ with open boundaries. The length of the line defect is $14a$. The zero-energy MSFs have tiny energy splitting due to the small size of the line defect, which is numerically found to be $<10^{-10}J$ for our parameters. (c) The amplitude of the mode function for γ_1 and γ_2. The black line indicates the line defect with chemical potential μ_d. The parameters are chosen as $\Delta=J$, $\mu_0=10J$, and $\mu_d=0.1J$.

Hamiltonian always remains gapped at any time as shown in Fig. 2(g), which protects the MSF modes from mixing with other modes. The evolution of the MSF modes γ_1 and γ_2 and their correlation are shown in Fig. 2(h). After the whole evolution with time T, apparently we have $\gamma_1(T)=\gamma_2(0)$ and $\gamma_2(T)=-\gamma_1(0)$. The correlation $\langle\gamma_1(T)\gamma_2(T)\rangle=-\langle\gamma_2(0)\gamma_1(0)\rangle=\langle\gamma_1(0)\gamma_2(0)\rangle$. This transformation of the MSF modes occurs in a similar way when we adiabatically braid the edges associated with different line defects. In Fig. 3(a), we illustrate the adiabatic braiding of two edge modes γ_2 and γ_3 of different line defects along a T-junction path. This braiding involves joining and cutting of two line defects and we need to choose parameters appropriately to avoid appearance of accidental near-zero-energy modes. In general, the four zero-energy MSF modes are still well protected by a significant energy gap. Their evolution and the associated correlations are shown in Fig. 3(b). The results indicate that $\gamma_2(T)=\gamma_3(0)$ and $\gamma_3(T)=-\gamma_2(0)$ for the two braided modes. The other modes remain unchanged with $\gamma_1(T)=\gamma_1(0)$ and $\gamma_4(T)=\gamma_4(0)$.

The above transformation rule generalizes straightforwardly to the case of $2N$ MSF modes. The rule is exactly the same as the case of Majorana fermions bound to vortices [24]. For $2N$ modes γ_j $(j=1,2,\ldots,2N)$, when we braid γ_j and γ_{j+1}, the transformation is described by a unitary operator $U_j=e^{\pi\gamma_{j+1}\gamma_j/4}$ which transforms $\gamma_j\to\gamma_{j+1}$ and $\gamma_{j+1}\to-\gamma_j$. As U_j and U_{j+1} do not commute, the exchange statistics of the MSF modes is non-Abelian and belongs to the

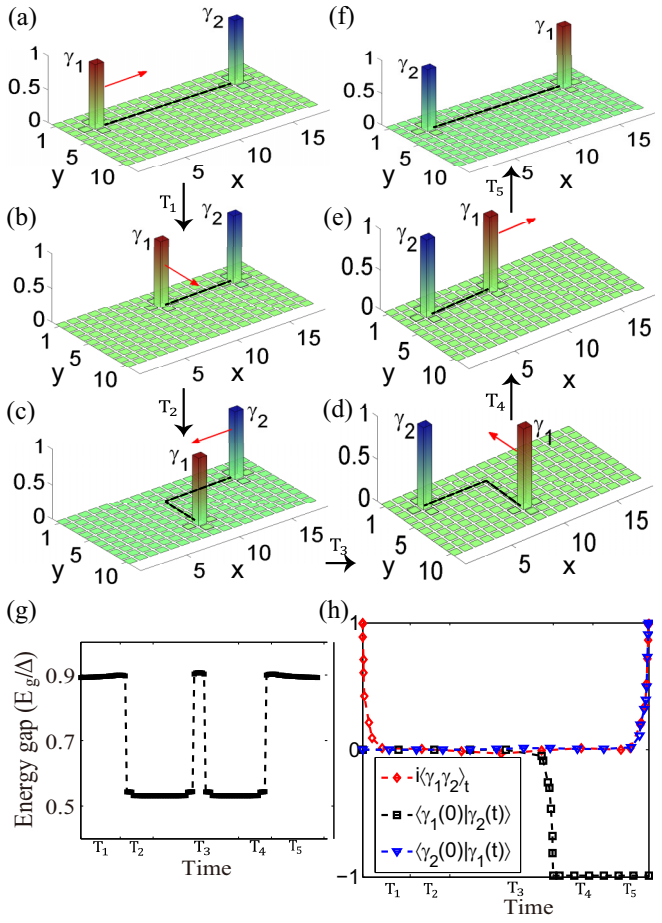

FIG. 2. (Color online) Braiding of two MSFs bound to the same line defect. (a) The black line indicates the line defect with chemical potential μ_d. Sequentially tuning the local chemical potentials at one end from μ_d to μ_0 shortens the line defect and transports γ_1 along the x direction. The red arrow shows the moving direction of the MSF. Similar operations along a T-junction path realize adiabatic exchange of γ_1 and γ_2, with steps illustrated in (a)–(f). (g) The evolution of the energy gap E_g throughout the braiding process. The system is always gapped with the minimum gap $E_g > 0.5J$. (h) Time evolution of the MSF modes γ_1,γ_2 and their correlations (see Appendixes A and B). All the parameters are the same as in Fig. 1. The total evolution time $T \sim 1.44 \times 10^4 J$.

so-called Ising anyon class according to the classification of non-Abelian anyons [42].

V. ROBUSTNESS TO REALISTIC IMPERFECTIONS

The unitary operation U_j from topological braiding of the MSF modes is robust against noise and experimental imperfections. To verify that, we examine several sources of noise typical for atomic experiments. First, with imperfect single-site addressing, when we tune the chemical potential of one site, we may change the potentials of the neighboring sites as well, modeled by a spreading ratio of $1-\alpha$. Second, there is a global weak harmonic trap for cold atom experiments, with an additional trapping potential $V_{\rm trap} = \frac{V_T}{2(L_x^2+L_y^2)} \sum_{\mathbf{r}} d_{\mathbf{r}}^2 c_{\mathbf{r}}^\dagger c_{\mathbf{r}}$, where L_x (L_y) is the lattice dimension along the x (y) direction, and $d_{\mathbf{r}}$ is the distance from the trap center. Typically,

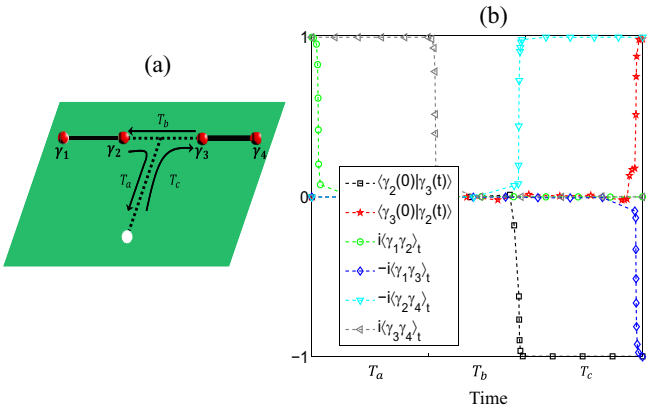

FIG. 3. (Color online) Braiding of two MSFs bound to different line defects. (a) Illustration of braiding two MSFs from different line defects along the T-junction path. (b) Time evolution of the MSF modes $\gamma_1,\gamma_2,\gamma_3,\gamma_4$ and their correlations. The MSFs γ_2 and γ_3 are braided. The parameters are taken as follows: the lattice size $12a \times 36a$, two horizontal line defects each of length $9a$ and distance $16a$, $\Delta = 0.91J$, $\mu_0 = 10\Delta$, and $\mu_d = 0.1\Delta$. The energy gap is also maintained during the braiding process $E_g > 0.5J$. The total evolution time $T \sim 1.92 \times 10^4 J$.

$V_{\rm T}$ ranges from $0.1J$ to J. Finally, there is unavoidable small disorder potential in experiments which adds random fluctuations to the chemical potential with magnitude denoted by λ_R. We recalculate the evolution of the MSF modes and their correlations, incorporating contribution of all these sources of noise. The results are shown in Fig. 4, which are almost indistinguishable from the corresponding results shown in Fig. 2(h) under the ideal case. This demonstrates the robustness of the braiding operations of the MSFs.

VI. DETECTION

To verify the non-Abelian braiding operations, we need to detect the topological qubit encoded by two nonlocal MSF modes γ_1 and γ_2. For the 1D nanowire, the parity of the total

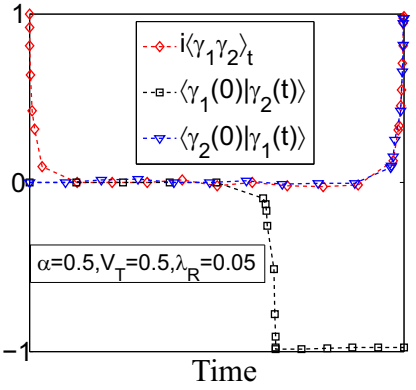

FIG. 4. (Color online) Robustness to experimental noise and imperfections. The lattice size is $20a \times 12a$ and other parameters are the same as in Fig. 1. α, V_T, λ_R denote the parameters characterizing respectively the laser beam crosstalk, the strength of the global harmonic trap, and the magnitude of random fluctuation of the chemical potential (see the main text). The total evolution time $T \sim 1.76 \times 10^4 J$.

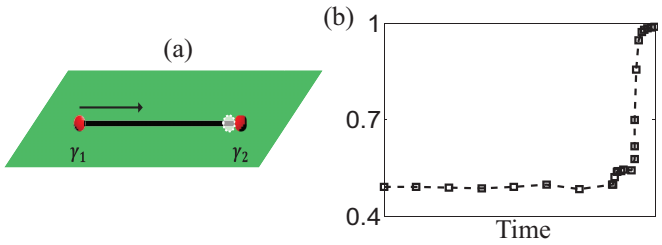

FIG. 5. (Color online) Detection of the topological qubit. (a) Two MSFs γ_1 and γ_2 are fused through adiabatic shortening of the line defect to a single lattice site $\mathbf{r}_0$. (b) Transformation of the MSF modes γ_1 and γ_2 under adiabatic merging. For simplicity, we plot evolution of the magnitude of the mode overlap between $c_{\mathbf{r}_0}$ and $[\gamma_1(t)+i\gamma_2(t)]/2$. At the end of merging, γ_1 and γ_2 are mapped dominantly to the local modes $c^\dagger_{\mathbf{r}_0}+c_{\mathbf{r}_0}$ and $i(c^\dagger_{\mathbf{r}_0}-c_{\mathbf{r}_0})$, respectively, which enables detection of the initial nonlocal topological qubit by a simple measurement of the atom number $c^\dagger_{\mathbf{r}_0}c_{\mathbf{r}_0}$ on a single lattice site after the adiabatic merging. All the parameters are the same as in Fig. 1. The total evolution time $T\sim 1.04\times 10^4 J$.

particle number is a conserved property, which is different for the two eigenstates of $i\gamma_1\gamma_2$ and thus can be used to detect the topological qubit [38,39]. For our case, the line defect interacts with the background lattice with tunneling and pairing terms which in general do not conserve the parity of the total atom number along the line; therefore, the parity detection does not work. We propose a different method to detect the topological qubit. The line defect is adiabatically shortened until it finally reduces to a single lattice site $\mathbf{r}_0$ [illustrated in Fig. 5(a)] and we examine evolution of the MSF modes γ_1 and γ_2 during this process. As shown in Fig. 5(b), with a high fidelity (about 99%), the mode γ_1 (γ_2) is mapped to $\gamma_{\mathbf{r}_0,A}=c^\dagger_{\mathbf{r}_0}+c_{\mathbf{r}_0}$ [$\gamma_{\mathbf{r}_0,B}=i(c^\dagger_{\mathbf{r}_0}-c_{\mathbf{r}_0})$], respectively. By a measurement of the local atom number $c^\dagger_{\mathbf{r}_0}c_{\mathbf{r}_0}$ after the adiabatic merging, we thus measure the topological operator $i\gamma_1\gamma_2$ with a high fidelity (about 98%). This local measurement is actually more robust compared with the nonlocal parity detection. Note that the detection fidelity of the topological qubit in principle can be improved to an arbitrary accuracy by using the quantum nondemolition (QND) technique: to measure the topological qubit $i\gamma_1\gamma_2$, we create an ancillary topological qubit (with MSF modes γ_3 and γ_4), perform an effective controlled-NOT gate between the topological qubits $i\gamma_1\gamma_2$ and $i\gamma_3\gamma_4$ through the noise-resilient braiding operations [8], and then measure the ancilla $i\gamma_3\gamma_4$ by the above method. As the qubit $i\gamma_1\gamma_2$ is not destroyed by the measurement, it can be repeatedly measured through this QND technique and the detection error is exponentially suppressed with increase of the detection rounds.

VII. DISCUSSION AND CONCLUSION

Our analysis is based on a concrete BdG Hamiltonian describing 2D $p+ip$ superconductors in the symmetry class D of the Periodic Table of topological insulators and superconductors [43,44], which lacks time-reversal symmetry. Ultracold atoms in optical lattices are capable of implementing more exotic topological phases that might harbor Majorana fermions. In the future, it might be interesting to explore whether MSFs exist as well in other symmetry classes and study their experimental realizations with cold atoms. In particular, one possible direction is to study MSFs in the DIII class, which has time-reversal symmetry and a Z_2 topological classification. As a consequence, Majoranas in this class should come in pairs at each end of the line defect due to Kramers's theorem and the braiding operations should always exchange two pairs of Majoranas. Whereas the non-Abelian statistics of Majorana Kramers's doublets in 1D DIII-class superconductor was theoretically demonstrated recently [45], the 2D case remains unexplored. Another important direction is to study the Shockley mechanism in 3D topological superconductors in symmetry class DIII and CI. In 3D, both DIII and CI class superconductors have time-reversal symmetry and a Z classification [43,44]. This study might lead to a promising experimental realization of 3D non-Abelian statistics as introduced by Teo and Kane [46].

In summary, we have proposed a complete scheme to observe non-Abelian statistics of the MSFs associated with line defects in a 2D optical lattice. The MSFs are created, braided, and fused all through adiabatic tuning of the chemical potential for certain lattice sites. The detection of the topological qubit is transformed to local measurement of the atom number on a single lattice site. The required technology fits well with the current status of the optical lattice experiments [31–35]. Through numerical simulation, we have demonstrated robustness of the non-Abelian braiding operations under a typical experimental configuration with imperfections. The scheme provides a viable approach for observation of the exotic non-Abelian braiding statistics, which is a goal of intense interest and a critical step for realization of robust topological quantum information processing [6–8].

ACKNOWLEDGMENTS

We thank J. Alicea, C. V. Kraus, and Y.-H. Chan for discussions. D.L.D., S.T.W., and L.M.D. are supported by the NBRPC (973 Program) Grant No. 2011CBA00300 (Grant No. 2011CBA00302), the IARPA MUSIQC program, the ARO, and the AFOSR MURI program. K.S. is supported in part by NSF Grant No. PHY-1402971.

APPENDIX A: TIME EVOLUTION

We first Fourier transform the Hamiltonian (1) into real space, with the modes in real space denoted by $c_{\mathbf{r}}$. A line defect has chemical potential μ_d instead of μ_0. We define the Majorana operators at each lattice site with $\gamma_{\mathbf{r},A}=(c^\dagger_{\mathbf{r}}+c_{\mathbf{r}})$ and $\gamma_{\mathbf{r},B}=i(c^\dagger_{\mathbf{r}}-c_{\mathbf{r}})$. In terms of these Majorana operators, the Hamiltonian has the following form:

$$H=\frac{i}{2}\sum_{\mathbf{p},\mathbf{q}}\mathcal{H}_{\mathbf{pq}}\gamma_{\mathbf{p}}\gamma_{\mathbf{q}}, \tag{A1}$$

where $p=(\mathbf{r},\beta)$ and $q=(\mathbf{r}',\beta')$ $(\beta,\beta'=A,B)$ are combined indices and $\mathcal{H}$ is a $2N\times 2N$ real skew-symmetric matrix with N being the number of lattice sites.

By locally and adiabatically tuning μ along a T-junction path, MSFs can be braided. During this process, the Majorana

operators evolve according to the following equation in the Heisenberg picture [47]:

$$\gamma_{\mathbf{p}} \rightarrow \gamma_{\mathbf{p}}(t) = U\gamma_{\mathbf{p}}(0)U^{\dagger} = \sum_{\mathbf{q}} \mathcal{O}_{\mathbf{qp}}\gamma_{\mathbf{q}}(0)\,, \tag{A2}$$

where $U = \mathcal{T}\exp[i\int_0^t H(\tau)d\tau]$ and $\mathcal{O} = \mathcal{T}\exp[-i\int_0^t \mathcal{H}(\tau)d\tau]$ is an element of the special orthogonal group $\mathcal{O} \in \mathrm{SO}(2N)$; $\mathcal{T}$ is the time-ordering operator.

In our numerical simulation, we first diagonalize $\mathcal{H}$ at time $t = 0$ to obtain the zero-energy eigenmodes $\gamma_i(0) = \sum_{\mathbf{p}} \eta_{i\mathbf{p}}\gamma_{\mathbf{p}}(0)$, where the coefficients $\eta_{i\mathbf{p}}$ represent the mode function and are localized at the ends of the line defects. During the braiding process, the zero-energy eigenmodes evolve as $\gamma_i(t) = U\gamma_i(0)U^{\dagger} = \sum_{\mathbf{p}} \eta_{i\mathbf{p}}\gamma_{\mathbf{p}}(t)$, where $\gamma_{\mathbf{p}}(t)$ are calculated via Eq. (A2). Using this method, we obtain the time evolution of the zero-energy MSF modes with the results plotted in the main text.

APPENDIX B: MAJORANA CORRELATION FUNCTIONS

To calculate the Majorana correlations, we use the method introduced in Ref. [48]. Let us define the density operator $\rho = N\exp(-\beta H)$ (N is the normalization constant and β is the inverse temperature) and the antisymmetric covariance matrix Γ with elements $\Gamma_{\mathbf{pq}} = \frac{i}{2}\mathrm{Tr}[\rho(\gamma_{\mathbf{p}}\gamma_{\mathbf{q}} - \gamma_{\mathbf{q}}\gamma_{\mathbf{p}})]$. The Hamiltonian H can be brought into block off-diagonal form $OHO^{\mathrm{T}} = \oplus_{j=1}^{N}\left(\begin{smallmatrix} 0 & -\epsilon_j \\ \epsilon_j & 0 \end{smallmatrix}\right)$ by a special orthogonal matrix $O \in \mathrm{SO}(2N)$, where ϵ_j characterizes the energy eigenspectrum of the Hamiltonian. This matrix O also reduces Γ to a block off-diagonal form $O\Gamma O^{\mathrm{T}} = \oplus_{j=1}^{N}\left(\begin{smallmatrix} 0 & \eta_j \\ -\eta_j & 0 \end{smallmatrix}\right)$ with $\eta_j = \tanh(\beta\epsilon_j/2)$. The covariance matrix Γ_{G} corresponding to the ground state of H is obtained by letting the inverse temperature $\beta \rightarrow \infty$, i.e., $\eta_j \rightarrow \mathrm{sgn}(\epsilon_j)$. After we obtain Γ_{G}, the Majorana correlations can be computed by Wick's theorem via the equation:

$$i\langle\gamma_{\mathbf{p}}\gamma_{\mathbf{q}}\rangle = \mathrm{Pf}(\Gamma_{\mathrm{G}}^{'}), \tag{B1}$$

where $\Gamma_{\mathrm{G}}^{'} = \left(\begin{smallmatrix} (\Gamma_{\mathrm{G}})_{\mathbf{pp}} & (\Gamma_{\mathrm{G}})_{\mathbf{pq}} \\ (\Gamma_{\mathrm{G}})_{\mathbf{qp}} & (\Gamma_{\mathrm{G}})_{\mathbf{qq}} \end{smallmatrix}\right)$ is a 2×2 submatrix of Γ_{G} and $\mathrm{Pf}(\Gamma_{\mathrm{G}}^{'})$ is the Pfaffian of $\Gamma_{\mathrm{G}}^{'}$ with $\mathrm{Pf}(\Gamma_{\mathrm{G}}^{'})^2 = \det(\Gamma_{\mathrm{G}}^{'})$. Once we have obtained $i\langle\gamma_{\mathbf{p}}\gamma_{\mathbf{q}}\rangle$ at time $t = 0$, the time evolution of the MSF mode correlations $i\langle\gamma_i\gamma_j\rangle_t$ can be computed directly using $\gamma_i(t) = \sum_{\mathbf{p}} \eta_{i\mathbf{p}}\gamma_{\mathbf{p}}(t) = \sum_{\mathbf{p},\mathbf{q}} \eta_{i\mathbf{p}}\mathcal{O}_{\mathbf{qp}}\gamma_{\mathbf{q}}(0)$.

[1] F. Wilczek, Nat. Phys. **5**, 614 (2009).
[2] A. Stern, Nature (London) **464**, 187 (2010).
[3] M. Z. Hasan and C. L. Kane, Rev. Mod. Phys. **82**, 3045 (2010).
[4] X.-L. Qi and S.-C. Zhang, Rev. Mod. Phys. **83**, 1057 (2011).
[5] J. Hisano, S. Matsumoto, and M. M. Nojiri, Phys. Rev. Lett. **92**, 031303 (2004).
[6] A. Y. Kitaev, Ann. Phys. (N.Y.) **303**, 2 (2003).
[7] C. Nayak, S. H. Simon, A. Stern, M. Freedman, and S. Das Sarma, Rev. Mod. Phys. **80**, 1083 (2008).
[8] D.-L. Deng and L.-M. Duan, Phys. Rev. A **88**, 012323 (2013).
[9] V. Mourik, K. Zuo, S. Frolov, S. Plissard, E. Bakkers, and L. Kouwenhoven, Science **336**, 1003 (2012).
[10] A. Das, Y. Ronen, Y. Most, Y. Oreg, M. Heiblum, and H. Shtrikman, Nat. Phys. **8**, 887 (2012).
[11] L. P. Rokhinson, X. Liu, and J. K. Furdyna, Nat. Phys. **8**, 795 (2012).
[12] M. Veldhorst, M. Snelder, M. Hoek, T. Gang, V. Guduru, X. Wang, U. Zeitler, W. van der Wiel, A. Golubov, H. Hilgenkamp *et al.*, Nat. Mater. **11**, 417 (2012).
[13] J. Alicea, Rep. Prog. Phys. **75**, 076501 (2012).
[14] C. Beenakker, Annu. Rev. Condens. Matter Phys. **4**, 113 (2013).
[15] E. J. Lee, X. Jiang, M. Houzet, R. Aguado, C. M. Lieber, and S. De Franceschi, Nat. Nanotechnol. **9**, 79 (2014).
[16] S. Nadj-Perge, I. K. Drozdov, J. Li, H. Chen, S. Jeon, J. Seo, A. H. MacDonald, B. A. Bernevig, and A. Yazdani, Science **346**, 602 (2014).
[17] J. Dalibard, F. Gerbier, G. Juzeliūnas, and P. Öhberg, Rev. Mod. Phys. **83**, 1523 (2011).
[18] I. Bloch, J. Dalibard, and S. Nascimbène, Nat. Phys. **8**, 267 (2012).
[19] M. Lewenstein, A. Sanpera, and V. Ahufinger, *Ultracold Atoms in Optical Lattices: Simulating quantum many-body systems* (Oxford University Press, Oxford, 2012).
[20] M. Sato, Y. Takahashi, and S. Fujimoto, Phys. Rev. Lett. **103**, 020401 (2009).
[21] S. Tewari, S. Das Sarma, C. Nayak, C. Zhang, and P. Zoller, Phys. Rev. Lett. **98**, 010506 (2007).
[22] S.-L. Zhu, L.-B. Shao, Z. D. Wang, and L.-M. Duan, Phys. Rev. Lett. **106**, 100404 (2011).
[23] N. Read and D. Green, Phys. Rev. B **61**, 10267 (2000).
[24] D. A. Ivanov, Phys. Rev. Lett. **86**, 268 (2001).
[25] A. Stern, F. von Oppen, and E. Mariani, Phys. Rev. B **70**, 205338 (2004).
[26] V. Gurarie, L. Radzihovsky, and A. V. Andreev, Phys. Rev. Lett. **94**, 230403 (2005).
[27] J. P. Gaebler, J. T. Stewart, J. L. Bohn, and D. S. Jin, Phys. Rev. Lett. **98**, 200403 (2007).
[28] Y.-J. Han, Y.-H. Chan, W. Yi, A. J. Daley, S. Diehl, P. Zoller, and L.-M. Duan, Phys. Rev. Lett. **103**, 070404 (2009).
[29] A. Bühler, N. Lang, C. V. Kraus, G. Möller, S. D. Huber, and H. P. Büchler, Nat. Commun. **5**, 4504 (2014).
[30] N. Syassen, D. M. Bauer, M. Lettner, T. Volz, D. Dietze, J. J. García-Ripoll, J. I. Cirac, G. Rempe, and S. Dürr, Science **320**, 1329 (2008).
[31] J. F. Sherson, C. Weitenberg, M. Endres, M. Cheneau, I. Bloch, and S. Kuhr, Nature (London) **467**, 68 (2010).
[32] C. Weitenberg, M. Endres, J. F. Sherson, M. Cheneau, P. Schauß, T. Fukuhara, I. Bloch, and S. Kuhr, Nature (London) **471**, 319 (2011).
[33] W. S. Bakr, J. I. Gillen, A. Peng, S. Fölling, and M. Greiner, Nature (London) **462**, 74 (2009).
[34] W. S. Bakr, A. Peng, M. E. Tai, R. Ma, J. Simon, J. I. Gillen, S. Foelling, L. Pollet, and M. Greiner, Science **329**, 547 (2010).
[35] P. Würtz, T. Langen, T. Gericke, A. Koglbauer, and H. Ott, Phys. Rev. Lett. **103**, 080404 (2009).

[36] M. Wimmer, A. R. Akhmerov, M. V. Medvedyeva, J. Tworzydło, and C. W. J. Beenakker, Phys. Rev. Lett. **105**, 046803 (2010).
[37] W. Shockley, Phys. Rev. **56**, 317 (1939).
[38] J. Alicea, Y. Oreg, G. Refael, F. von Oppen, and M. P. Fisher, Nat. Phys. **7**, 412 (2011).
[39] C. V. Kraus, P. Zoller, and M. A. Baranov, Phys. Rev. Lett. **111**, 203001 (2013).
[40] L. Fu and C. L. Kane, Phys. Rev. Lett. **100**, 096407 (2008).
[41] J. D. Sau, R. M. Lutchyn, S. Tewari, and S. Das Sarma, Phys. Rev. Lett. **104**, 040502 (2010).
[42] P. Di Francesco, D. Sénéchal, and P. Mathieu, *Conformal Field Theory* (Springer, New York, 1997).
[43] A. P. Schnyder, S. Ryu, A. Furusaki, and A. W. W. Ludwig, Phys. Rev. B **78**, 195125 (2008).
[44] A. Kitaev, in *Periodic Table for Topological Insulators and Superconductors*, AIP Conf. Proc. No. 1134 (AIP, New York, 2009), p. 22.
[45] X.-J. Liu, C. L. M. Wong, and K. T. Law, Phys. Rev. X **4**, 021018 (2014).
[46] J. C. Y. Teo and C. L. Kane, Phys. Rev. Lett. **104**, 046401 (2010).
[47] C. V. Kraus, M. M. Wolf, and J. I. Cirac, Phys. Rev. A **75**, 022303 (2007).
[48] C. V. Kraus, M. M. Wolf, J. I. Cirac, and G. Giedke, Phys. Rev. A **79**, 012306 (2009).